JOURNAL OF PROPULSION AND POWER
Vol. 11, No. 5, September–October 1995

# Characteristics of a Velocity-Modulated Pressure-Swirl Atomizing Spray

Fumiaki Takahashi* and W. John Schmoll†
*University of Dayton, Dayton, Ohio 45469*
and
John L. Dressler‡
*Fluid Jet Associates, Spring Valley, Ohio 45370*

**The liquid spray from a production pressure-swirl atomizing nozzle, attached to a novel high-amplitude piezoelectric driver, has been characterized using phase-Doppler anemometry and visualization techniques. The high-amplitude velocity modulation of the hollow-cone liquid jet induced the collisions of consecutive segments of the liquid sheet, resulting in coherent roll-up and breakup processes in a wide range of the modulation frequency (ca. 4–52 kHz). Two distinct breakup modes were found at different resonant frequencies: ~17 and ~19 kHz. At the former frequency, the liquid sheet (cone) atomized and bifurcated in two major directions, dispersing the droplets more evenly; at the latter frequency, the driver's pumping action induced atomization near the nozzle exit, accelerated the droplets primarily in the core region, and narrowed the spray angle with increasing driving power. The driver was able to improve spray quality, even at a low pressure of 207 kPa (compared to a normal operating pressure of 690 kPa). Thus, the atomizer is promising to throttle the liquid flow rate and increase the turndown ratio.**

## Introduction

PRESSURE-SWIRL atomizers are commonly used in a variety of practical devices, including propulsion and power systems such as gas-turbine combustors, and industrial and domestic burners. A major design problem of such atomizers is achieving good atomization over a range of fuel flow rates in which the maximum-to-minimum (turndown) ratio may reach 40.[1] The operational flow rate range is bounded by poor spray characteristics at low flows (or pressures) and excessive pressures at high flows. Furthermore, because the swirl slot and orifices in the pressure-swirl atomizing nozzles are small and tend to clog, the nozzles designed for low fuel flow rates (<0.8 cc/s) are not always reliable.[2] Therefore, if the spray quality were improved at low flow rates, the turndown ratio would be increased dramatically.

Ultrasonic atomizers, developed for low fuel flow rates, are particularly suitable for domestic oil burners.[2,3] The ultrasonic atomizers utilize a vibrating surface, which generates waves on the liquid surface. The crests of these waves break and form droplets; the higher the frequency, the smaller the droplets. This technique is advantageous for atomization at low flow rates because relatively large fuel-feed passages can be used in the atomizer. However, the droplet velocity from an ultrasonic atomizer is low compared with that of a pressure atomizing spray; thus, droplet penetration into the airstream is less.

An important issue in practical systems, in general, is the uniformity of the spray. The pressure-swirl atomizer forms a hollow-cone liquid sheet that is subjected to the Kelvin–Helmholtz instability[4–7] and eventually atomizes. This instability is convective; i.e., it grows in space with respect to an observer sitting on the system. The instability causes the sheet to flap and segment sporadically; consequently, the droplets tend to be concentrated in packets (or clusters), thereby making the spray spatially and temporally nonuniform.[8] The clusters of droplets were observed in a spray produced by a gas-turbine combustor swirl-cup atomizer,[9] in which a pressure-swirl atomizing spray impinged on a venturi surface to form a thin film for secondary atomization by high-shear counterswirl airflow. The combustion of these clusters can lead to periodic variations in the heat-release rate and pressure in the combustor and, in turn, may result in various combustion problems such as combustion roar, combustion-driven oscillations, formation of various pollutants, and even lower combustion efficiency.[10] Therefore, if the nonuniform atomization were eliminated, the combustion characteristics would be greatly improved.

An atomizer, based on the mechanism of high-amplitude velocity-modulation, has recently been developed.[8,11,12] It can generate either monodisperse droplet arrays or polydisperse sprays, depending on the power supplied to the piezoelectric driver. The liquid jet to be atomized can be in various forms such as circular or square column, flat sheet, and conical sheet. Because of the unique atomization process, droplet generation or spray atomization can be induced in a wide range of modulation frequencies. The velocity-modulation atomizer has recently[13] been characterized for a single-column jet with a circular or rectangular orifice. In this article, the piezoelectric driver is used to stimulate a hollow-cone liquid sheet produced by a production pressure-swirl atomizer. An attempt is made to gain a better understanding of the velocity-modulation atomization process and its impact on the characteristics of practical pressure-swirl atomizing sprays. The phase-Doppler anemometry and two visualization techniques were used to characterize the spray.

## Experimental Techniques

The high-amplitude velocity-modulation atomizer assembly (Fig. 1) consists of a piezoelectric crystal driver in a circular housing, described in detail elsewhere,[8,11–13] and a pressure-swirl atomizer (Delavan; hollow-cone type, 60-deg spray angle, 2.1 cc/s nominal flow rate at 690-kPa gauge pressure)

Presented as Paper 94-0558 at the AIAA 32nd Aerospace Sciences Meeting and Exhibit, Reno, NV, Jan. 10–13, 1994; received Jan. 31, 1994; revision received Nov. 8, 1994; accepted for publication Nov. 13, 1994. 

*Research Engineer, Research Institute, 300 College Park. Senior Member AIAA.
†Associate Research Physicist, Research Institute.
‡Owner, 1216 Waterwyck Trail.

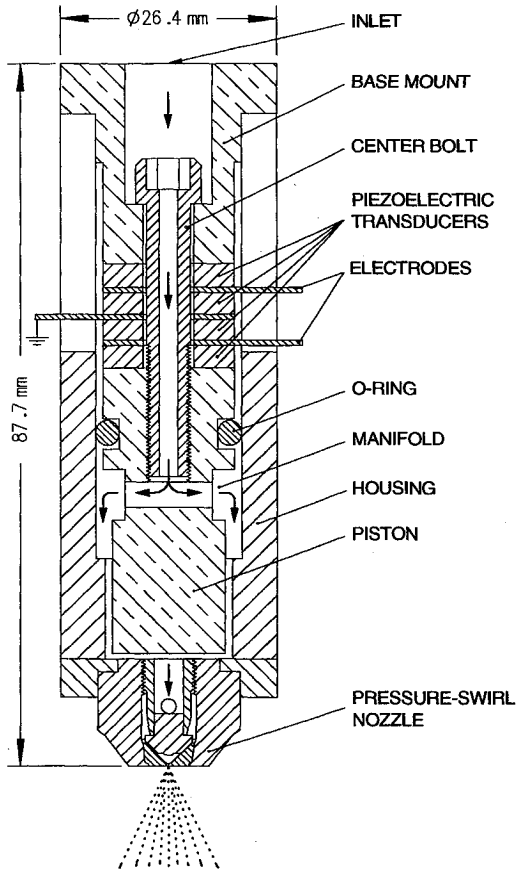


**Fig. 1 Atomizer assembly.**

across the end of the housing. The diameter and length of the atomizer are 26.4 and 87.7 mm, respectively. The working fluid is introduced into the central passage, distributed around a piston by a manifold, and discharged from the pressure-swirl nozzle. The model of the current atomizer contains four functional elements: 1) the piezoelectric transducers that receive the electrical signal and convert it to longitudinal mechanical motion, 2) a mechanical structure that amplifies the motion produced by the transducers, 3) a pump that converts the amplified mechanical motion to a pressure perturbation in the working fluid, and 4) a nozzle that creates a hollow-cone fluid sheet whose velocity is modulated by the pressure perturbation.

The mechanical structure is a cylindrical assembly including the transducers (EDO Corp.) and the piston, which are combined together and secured to a base mount with a hollow center bolt. By using a transducer pair and applying the driving voltage to the center electrode (the piston and housing are held at ground potential), the probability of an electric short circuit is reduced. In the driver used in this article, two pairs of piezoelectric transducers are incorporated in the structure to augment the longitudinal displacement. The mechanical structure is a resonant device that can exhibit large mechanical deflections at specific resonant frequencies. At these resonances, the motion produced by the transducers is amplified at the end of the piston because the length of the mechanical structure is several times the total thickness of the transducers. Furthermore, the current and voltage to the piezoelectric transducer are in phase at these resonant frequencies; thus, energy loss in the electrical power amplifier is minimized. The narrow passage around the piston, defined by the housing and an end plate, constitutes the pump. Unlike other ultrasonic atomizers[14,15] that have fluid manifolds designed to be resonant at the operating frequency, the pump in this device does not have a resonance at the operating frequency.

The atomizer assembly is attached to a three-dimensional translational stage incorporating magnetic scales with 5-$\mu$m-precision digital indicators. The test fluid[8] is distilled water with a small fraction of additives (ethylene glycol, 1.0%; preservative [Givaudan Corp., Giv-Gard DXN], 0.1%; sodium borate decahydrate, 0.1%; sodium nitrite, 0.1%; benzotriazole, 0.01%; concentrated NaOH, trace for pH adjustment to 8.1), to make the fluid noncorrosive and sterile (measured surface tension: 69.4 dyne/cm at 21°C). Figure 2 shows a block diagram of the experimental setup. Compressed air at the supply tank gauge pressure $P_t$ forces the liquid to the atomizer. The fluid is sprayed downward through the atmosphere into a large collector (45 cm diameter × 60 cm height), with a suction line that creates an airflow just sufficient to prevent the droplets from drifting backward.

The velocity modulation system includes a function generator (Wavetek 22), power amplifier (Denon POA-2200), matching transformer, and piezoelectric transducers. The sinusoidal driving signal with the peak-to-peak voltage $V_{p\text{-}p}$ and frequency $f$ is applied to the center electrode of the piezoelectric transducers. The peak-to-peak current $I_{p\text{-}p}$ depends on the crystal response. Both $V_{p\text{-}p}$ and $I_{p\text{-}p}$ are measured by an oscilloscope (Tektronix 2205).

The droplet diameter and velocity are measured by a two-component phase-Doppler anemometer (Aerometrics), which consists of a transmitting optic system, receiving optic system, and counter-type processor. An argon-ion laser (Coherent Innova 200; typical operating output: 0.3–0.6 W) is the light source. The calculated fringe spacings of the 514.5- and 488-nm beams are 6.7 and 6.2 $\mu$m, respectively. The beam waist diameter at the beam crossing is approximately 90 $\mu$m. The scattering light from a droplet is detected by the receiver at a 30-deg-off-axis forward-scattering mode. The number of samples at each location is typically 4000, except for the peripheral region of a spray where the data rate drops significantly. It has been known[16,17] that the phase-Doppler measurements are sensitive to user-controlled settings, particularly photomultiplier tube (PMT) voltage. To maintain the consistency in the setting, the data presented in this article were acquired using the automated PMT voltage setting, provided by the manufacturer's software (PDPA version 4.27B). Basically, the voltage is adjusted, after several trial runs, to a value that is high enough to detect small droplets, yet low enough to avoid the saturation of the PMT at each location in the spray.

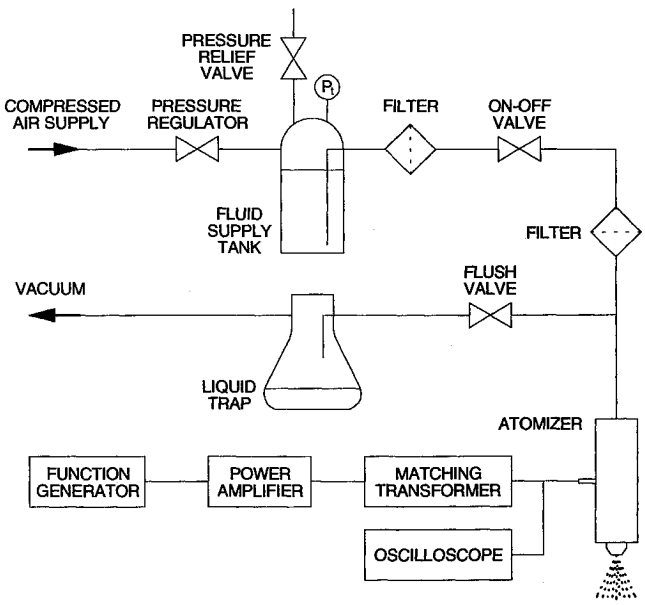


**Fig. 2 Experimental setup.**

## Results and Discussion

### Optical Observations

Photographic and high-speed cinematographic observations were made using two types of lighting methods: 1) backlighting (stroboscope or flood lamp) and 2) continuous-wave laser-sheet (argon-ion laser at an output of 23 W). Figure 3 shows back-lit stroboscopic photographs of the sprays with and without driving at $P_t$ = 690 kPa. The spray with no driving (Fig. 3a) shows a liquid sheet with the development of waves due to the Kelvin–Helmholtz instability,[4–7] eventually disintegrating into droplets. The waves of the liquid sheet are asymmetric and their shape seems random. The occasional disintegration of liquid sheet segments, which is then atomized, appears to cause droplets to group into clusters. By using a fast Fourier transform (FFT) analysis of the time-of-arrival data in the phase-Doppler measurement, Bachalo et al.[18] investigated the pressure atomizing spray. They found that the dominant frequency of the clusters was 55 Hz if the spray was in a swirling airflow and that droplet arrival was essentially random without the airflow. Because liquid-sheet disintegration occurs randomly, the time-of-arrival data analysis may not be able to resolve the droplet clustering due to the instability of the liquid sheet.

At the driving frequency $f$ = 5 kHz (Fig. 3b), the conical liquid sheet rolled up into a circular ligament that traveled downstream and shortened the sheet length (cf. Fig. 3a), thus preventing further growth of the natural instability. As a result, atomization occurred in a more symmetric and controlled manner. As the driving frequency increased (Figs. 3c–3e), multiple coherent rolled-up waves, or ligaments, appeared before atomization. Consequently, the liquid volume in each circular ligament (and droplet cluster) decreased. Notice that the driving frequencies are orders of magnitude larger than that of the clustering by the airflow.[18]

Figures 3e and 3f compare two cases with different applied voltage (or power) at a fixed resonant frequency (~19 kHz), at which the current decreased slightly compared to adjacent frequencies. If the power is low (Fig. 3e), the structure of the liquid sheet and spray looks similar to those observed at lower frequencies (Figs. 3b–3d). However, if the power is high (Fig. 3f) with the voltage the same as Figs. 3c and 3d, the atomization process changes dramatically; atomization appears to take place near the nozzle exit.

The laser-sheet planar visualization was made in the vertical plane, including the axis, and horizontal planes at different axial distances from the nozzle [$x$ = 20 mm, 60 mm (not shown), and 100 mm (not shown)]. Figure 4 shows the exposure (1/250 s) photographs of the sprays with and without driving. The vertical tomogram for the no-driving case (Fig. 4a) clearly shows a liquid sheet (bright linear zone) that atomizes into droplets at the distance along the sheet from the nozzle exit $l \approx 7$ mm. In the periphery of the spray downstream, some droplets were quickly curved inward (more noticeable in the right half), while others kept going straight. This trend shows that smaller drops are entrained by the spray-induced flow into the internal region after losing their momentum and larger drops with a higher momentum continue their straight trajectories.

The horizontal tomogram at $x$ = 20 mm (Fig. 4b) exhibits the "hollow-cone" structure (bright circle) of the spray. Here, the time-exposure photographs of sprays need to be interpreted carefully because of the spatial variations in the droplet number density, size distribution, and velocities. The area of

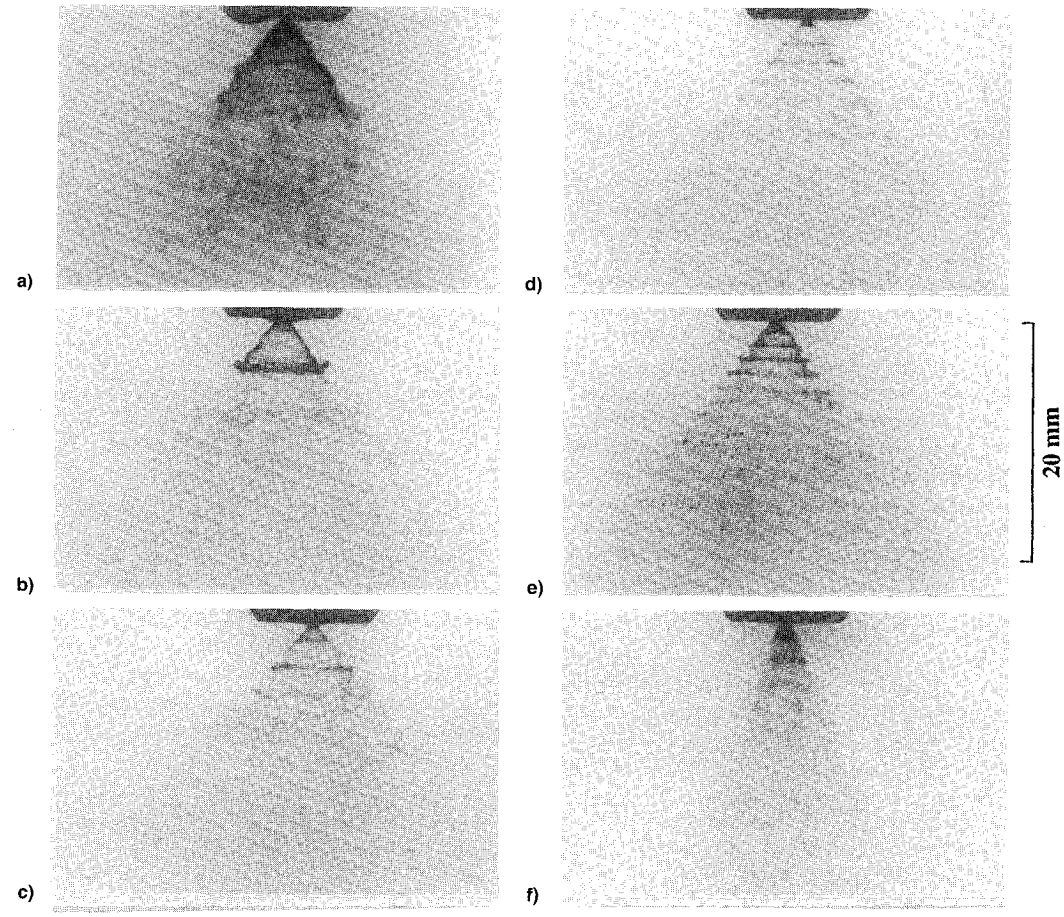


**Fig. 3 Back-lit stroboscopic photographs. $P_t$ = 690 kPa: a) no driving; b) $f$ = 5 kHz, $V_{p\text{-}p}$ = 800 V, $I_{p\text{-}p}$ = 40 mA; c) $f$ = 10 kHz, $V_{p\text{-}p}$ = 1400 V, $I_{p\text{-}p}$ = 160 mA; d) $f$ = 15 kHz, $V_{p\text{-}p}$ = 1400 V, $I_{p\text{-}p}$ = 260 mA; e) $f$ = 19.2 kHz, $V_{p\text{-}p}$ = 340 V, $I_{p\text{-}p}$ = 100 mA; and f) $f$ = 19.1 kHz, $V_{p\text{-}p}$ = 1400 V, $I_{p\text{-}p}$ = 260 mA.**

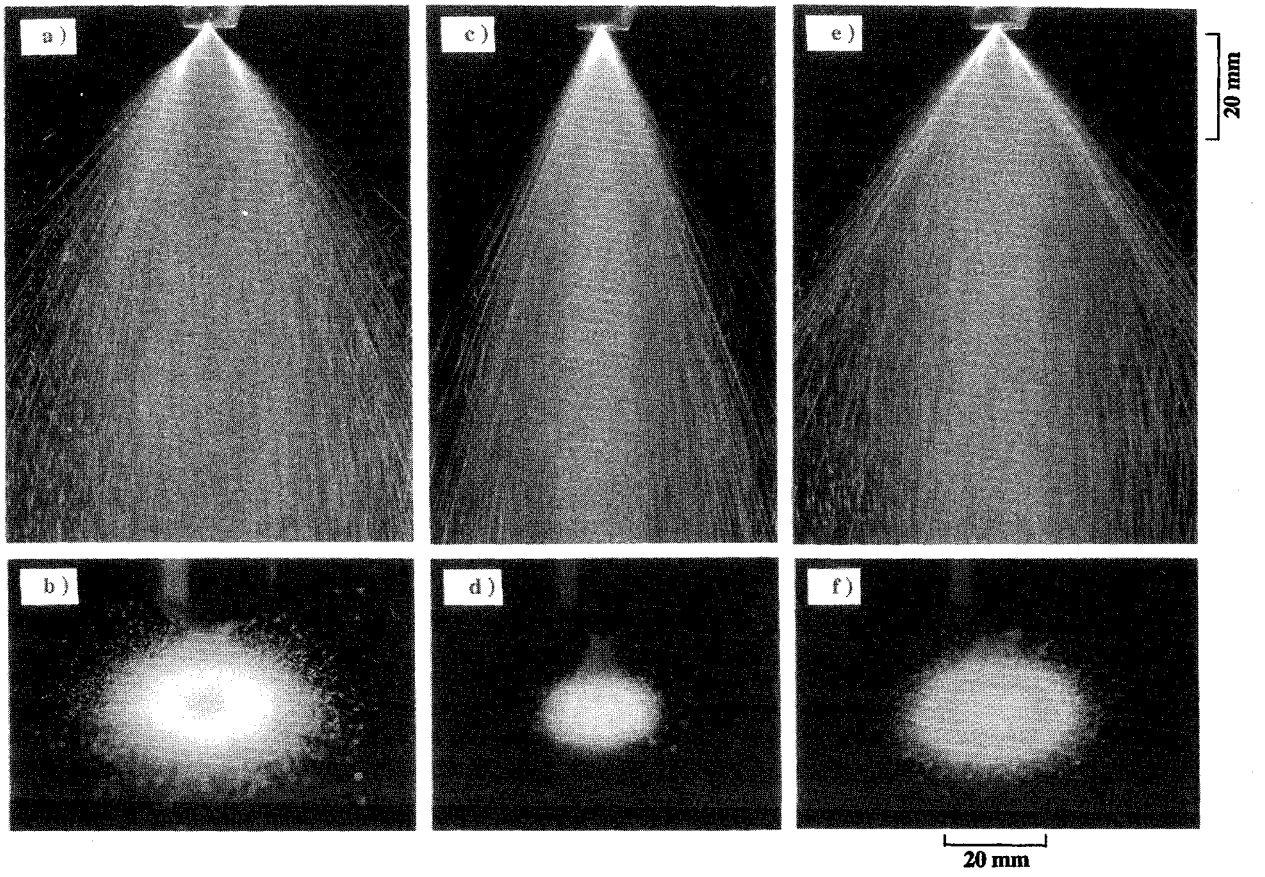


**Fig. 4 Laser-sheet planar visualization photographs. Exposure: 1/250 s. $P_t$ = 690 kPa: a) and b) no driving; c) and d) $f$ = 19.0 kHz, $V_{p\text{-}p}$ = 1000 V, $I_{p\text{-}p}$ = 184 mA; e) and f) $f$ = 19.0 kHz, $V_{p\text{-}p}$ = 1500 V, $I_{p\text{-}p}$ = 300 mA.**

high-volume flux appears to be bright regions in the photograph because of the scattering from multiple droplets passing during the exposure period as well as the high-intensity scattering from large particles. However, even if the volume flux is small (such as the area where low-speed small droplets are drifting), the scattering light is recorded in the film. For this reason, the central region of the hollow-cone-type spray is not completely dark in the photograph.

For a high driving power (1500 V, 300 mA) at ~19 kHz (Figs. 4c and 4d), the bright hollow-cone sheet near the nozzle and a bulb-like atomization region (Fig. 4a) were no longer observed, and the atomization appeared to occur right after the nozzle exit. As a result, a dense core was formed and the spray angle decreased. On the other hand, at another resonant frequency (~17 kHz; Figs. 4e and 4f), at which the current increased slightly compared to adjacent frequencies, atomization occurred after a hollow-cone sheet was formed, similar to the no-driving case (Fig. 4a), but at a location closer to the nozzle ($l \approx 4$ mm). The droplet stream is apparently bifurcated in two major directions [i.e., along the conical surface and inward (Fig. 4e)], dispersing the droplets more evenly (Fig. 4f). At this frequency, the spray angle did not change at a higher power ($V_{p\text{-}p}$ = 1500 V, $I_{p\text{-}p}$ = 320 mA; not shown). High-speed (10,000 fps) cinematography (not shown) was helpful in interpreting the still photographs, although it was not able to resolve the atomization process completely.

Although there are some ambiguities in determining the exact locations of the liquid sheet and roll-up waves, quantitative information can be retrieved from the back-lit stroboscopic photographs. Figure 5 shows the wavelength of the roll-up waves $\lambda$ measured along the liquid sheet, the wave transit velocity $\lambda \times f$, and the cone apex angle $2\theta$ as a function of the driving frequency at $P_t$ = 690 kPa. The data points of these variables at 10 kHz show that the effect of the driving power is negligible except for the driver's second resonant

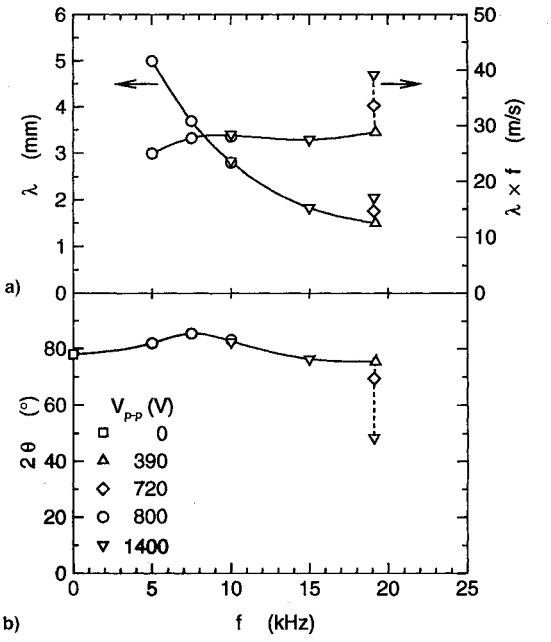


**Fig. 5 Variations in a) wavelength, transit velocity and b) cone angle with the driving frequency. $P_t$ = 690 kPa.**

frequency (~19 kHz). The wavelength decreased almost inversely with increasing the driving frequency; thus, the wave transit velocity was nearly constant (~28 m/s). The cone angle varied slightly from its no-driving value (78 deg) with driving frequency, but the variation was not significant. By contrast, at the resonant frequency, the wavelength and velocity increased and the cone angle decreased dramatically (approximately 36% for all variables) by increasing the driving power

(from 390 V, 100 mA to 1400 V, 200 mA). Apparently, the driver's pumping action accelerated the liquid jet velocity, and large velocity fluctuations caused atomization near the nozzle exit, narrowing the spray cone angle (Figs. 3f and 4c).

#### Velocity-Modulation Atomization

While it has long been known[4-7] that atomization in the pressure-swirl spray occurs as a result of the natural instability and breakup processes, the atomization process under high-power stimulation by the current piezoelectric driver is dominated by a totally different mechanism, which we call[13] the "velocity-modulation atomization." Figure 6 shows conceptual sketches of the atomization processes for a single-column jet and a conical sheet. In the low-power (Rayleigh breakup) mode in a single jet (Fig. 6a), the piezoelectric driver only establishes periodic boundary conditions for the capillary instability, which then breaks the cylindrical liquid jet into a stream of monodisperse drops. In the high-power mode (Fig. 6b), sufficiently energetic velocity modulation of the liquid is employed to generate large surface perturbations that break the liquid jet into a spray. Unlike conventional Rayleigh-breakup monodisperse droplet generators[19-23] or conventional ultrasonic atomizers,[2,3] which use the mechanical vibration of the nozzle, this atomizer directly generates a high-amplitude velocity perturbation of the liquid flow. The atomization mechanism is similar to that produced by impinging jets,[24] except here all the liquid emerges from the same nozzle. Sections of the fluid jet, moving at different relative velocities, collide; this impact creates radial velocity perturbations, forms circular discs, and atomizes the fluid.

In the velocity-modulated hollow-cone liquid jet, segments of the liquid sheet possess a velocity fluctuation whose sign changes alternatively (Fig. 6c). Thus, the collisions of segments of liquid sheet result in roll-up of the sheet (if the modulation is moderate), create circular waves (or ligaments), then break up into droplets. The formation of the ligaments and atomization were observed (Figs. 3b–3e) in a wide range of the modulation frequency (4–52 kHz). The characteristics of the spray changed significantly at the piezoelectric driver's resonant frequency (~19 kHz), at which the mechanical deflections were so large that the magnitude of velocity modulation might be comparable to the average velocity. Consequently, the high-power pumping action induced large collisions in the vicinity of the nozzle exit; thus, atomization occurred before a thin conical sheet formed (Figs. 3f and 4c). On the other hand, the bifurcated atomization process observed at $f \approx 17$ kHz (Fig. 4e) apparently occurred at a certain distance ($\sim 2\lambda$) from the nozzle along the sheet. Although critical conditions that determine the occurrence of these different atomization processes have not yet been revealed, the velocity-modulation amplitude relative to the average liquid sheet velocity must be a decisive factor. Therefore, the piezoelectric driver's electromechanical responses near the resonance frequencies must play a key role.

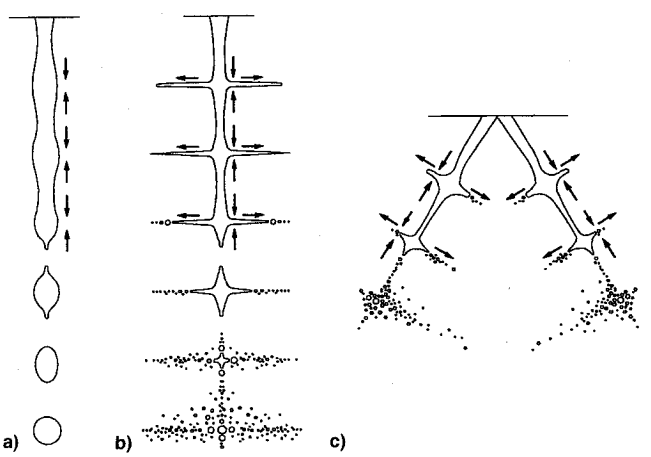


**Fig. 6 Conceptual sketches of the velocity-modulation atomization processes: a) single jet, low-power (Rayleigh breakup) mode; b) single jet, high-power mode; and c) hollow-cone jet. Arrows indicate the directions of the velocity fluctuation.**

#### Phase-Doppler Anemometry Measurements

The experimental conditions for the phase-Doppler measurements are shown in Table 1, which also includes the cross-sectional average diameters that will be explained later. The results for the base case at $P_t = 690$ kPa with no driving (run 1) will be presented first, and the effects of the driving power (runs 2, 3, and 3*), the driving frequency (run 4), and the atomizing pressure (runs 5 and 6) will be examined.

Figure 7a shows the radial profiles of the (validated) data rate (D.R.) of the phase-Doppler measurement (which approximately represents the droplet number flux), with the probability density functions (pdf) of the droplet diameter at selected locations at three different axial distances from the nozzle for the no-driving case (run 1). At $x = 20$ mm, the data rate showed double peaks that reached ~2600 Hz at the transverse distance from the axis $y \approx \pm 8$ mm, and the spray was bounded at $y \approx \pm 22$ mm. This result is consistent with the horizontal laser-sheet photograph (Fig. 4b), which shows the hollow-cone nature of the spray. At downstream locations, the peak values decreased (and two peaks merged at $x = 100$ mm) and the spray boundary spread, as expected. The pdf shifted toward larger droplet diameters outwardly or downstream. Figure 7b shows the radial profiles of the arithmetic mean droplet diameter

$$\left(D_{10} = \sum_{i=1}^{N} d_i/N\right)$$

where $d_i$: diameter of $i$th droplet; $N$: total number of sample, and Sauter mean droplet diameter

$$\left(D_{32} = \sum_{i=1}^{N} d_i^3 \Big/ \sum_{i=1}^{N} d_i^2\right)$$

At $x = 20$ mm, $D_{10}$ was minimum (~8 $\mu$m) on the centerline and increased outwardly to ~40 $\mu$m at the spray periphery ($y \approx \pm 22$ mm). $D_{32}$ was larger (13–70 $\mu$m), typical of polydispersed sprays, because it reflected the volume (and surface area) of the droplets, thereby weighting more on larger drops. As the spray spread out downstream ($x = 60$ mm, 100 mm), the maximum values of both $D_{10}$ and $D_{32}$ in the spray periphery increased. This result is consistent with the optical observation that the smaller droplets in the peripheral region tend to be entrained inwardly and the larger droplets tend to remain in the region as described before.

Figure 7c shows the mean axial $U_d$ and radial $V_d$ droplet velocity components. At $x = 20$ mm, $U_d$ had double peaks (~11 m/s) at $y \approx \pm 12$ mm, slightly outside the data-rate peaks, and $V_d$ reached its maximum (~8 m/s) further outside ($y \approx \pm 20$ mm) the $U_d$ peaks. At downstream locations ($x = 60$, 100 mm), the magnitudes of both $U_d$ and $V_d$ decreased as the droplets lost their momenta due to drag forces. Figure 7d shows the mean droplet trajectory angle $\alpha_d$ with respect to the $x$ axis, determined by taking an average of the individual trajectory angle calculated from the velocity components. At $x = 20$ mm, the radial locations at which $2|\alpha_d| \approx 60$ deg (nominal spray angle) were coincident with the peak locations ($y \approx \pm 15$ mm) of the total mean droplet velocity ($\sqrt{U_d^2 + V_d^2}$). For the droplets in the periphery, where the data rate vanished, $2|\alpha_d|$ reached ~100 deg at $x = 20$ mm and decreased downstream to ~60 deg at $x = 100$ mm.

Figure 8 shows the effect of driving at different power levels and frequencies at $P_t = 690$ kPa, measured at $x = 20$ mm.

**Table 1 Experimental conditions and cross-sectional average diameters**

| Run | $P_t$, kPa | $f$, kHz | $V_{p\text{-}p}$, V | $I_{p\text{-}p}$, mA | $\bar{D}_{10}$, $\mu$m | $\bar{D}_{32}$, $\mu$m |
|---|---|---|---|---|---|---|
| 1 | 690 | — | No driving | — | 26 | 60 |
| 2 | 690 | 19.1 | 1000 | 184 | 24 | 50 |
| 3 | 690 | 19.3 | 1400 | 224 | 23 | 49 |
| 3*[a] | 690 | 18.9 | 1500 | 290 | — | — |
| 4 | 690 | 17.1 | 1000 | 240 | 22 | 55 |
| 5 | 207 | — | No driving | — | 42 | 97 |
| 6 | 207 | 19.1 | 1000 | 184 | 37 | 93 |

[a]Run 3* is for the axial scan only (Fig. 9).

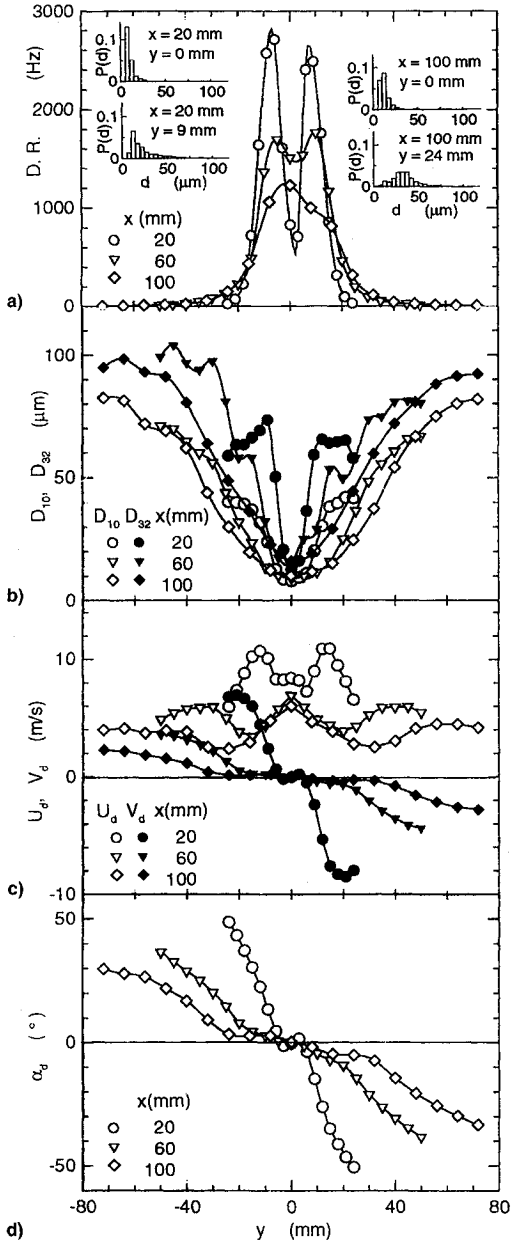


**Fig. 7 Radial profiles of a) data rate, b) mean droplet diameters, c) velocity components, and d) mean trajectory angle. No driving (run 1). $P_t$ = 690 kPa.**

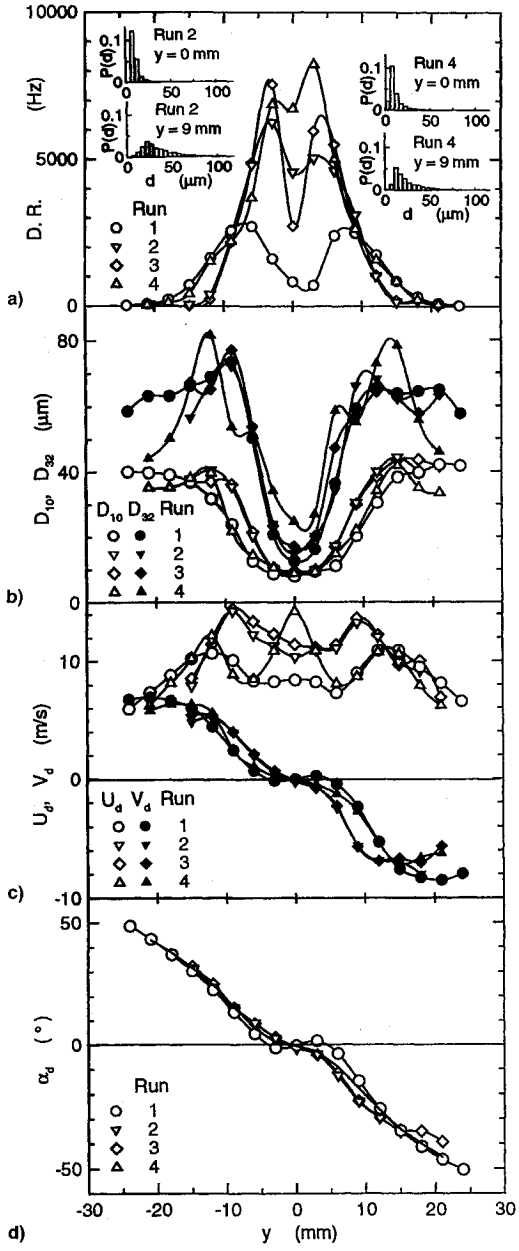


**Fig. 8 Effect of driving power and frequency on the radial profiles a) data rate, b) mean droplet diameters, c) velocity components, and d) mean trajectory angle. $P_t$ = 690 kPa, $x$ = 20 mm.**

For $f \approx 19$ kHz, the peak values of the data rate increased more than twice with an increase in the driving power (runs 2 and 3 in Fig. 8a), compared to the no-driving case (run 1), and the distribution narrowed. This finding is consistent with the measurement of the cone angle (Fig. 5b) that the spray angle became narrower with driving. At $f \approx 17$ kHz (run 4), the data rate showed a peculiar distribution, i.e., high data-rate peaks (nearly three times that of run 1) similar to driving at 19 kHz (runs 2 and 3) in the central region ($-10 < y < 10$ mm) and a distribution nearly identical to the no-driving case (run 1) in the outer region ($|y| > 10$ mm). Thus, the bifurcated atomization process threw droplets into the core region at high rates, while it maintained the droplet number flux the same as the no-driving spray in the periphery. Figure 8b shows the mean diameter distributions. The profile of $D_{10}$ for run 4 followed almost exactly the no-driving case (run 1)

in $-10 < y < 10$ mm, while the profiles for runs 2 and 3 were significantly narrower. The profile of $D_{32}$ for run 4 showed a peculiar deviation from the curve for the no-driving case because of the changes in the pdf as a result of the bifurcated atomization.

To assess the influence of driving on the droplet diameter in a global manner, the spray cross-sectional average diameters ($\bar{D}_{10}$, $\bar{D}_{32}$) were calculated by taking area averages of $D_{10}$ and $D_{32}$ from the centerline to the spray periphery with the data rate as the weighting factor. Although this procedure is somewhat crude (since it does not take into consideration the dependency of the probe cross-sectional area on the droplet diameter), it requires only principal variables ($D_{10}$, $D_{32}$, and D.R.), which are less sensitive to the instrument settings and the flowfield than the derived variables (the number density and volume flux), and thus, more reproducible. Furthermore, the procedure is probably sufficient to evaluate the differences due to excitation of the driver. Table 1 lists the results of the averages for all cases. As a result of driving, $\bar{D}_{10}$ and $\bar{D}_{32}$ decreased ~8 and ~17%, respectively, for run 2; ~12 and ~18%, respectively, for run 3; and ~15 and ~8%, respectively, for run 4. These changes are considered to be significant and should be greater than the measurement error.

The mean axial and radial droplet velocity distributions (Fig. 8c) show striking differences due to the driving conditions. For $f \approx 19$ kHz (runs 2 and 3), both $U_d$ and $V_d$ at two different power levels were nearly identical, and $U_d$ was ~40% greater than the no-driving case (run 1) in the central region ($-10 < y < 10$ mm). This result is reasonable compared to the increase in the wave transit velocity with the driving power described earlier (Fig. 5a). By contrast, for $f \approx 17$ kHz (run 4), $U_d$ exhibited peculiar distributions. The $U_d$ profile was close to the no-driving case, except for the near-axis region ($-5 < y < 5$ mm), where $U_d$ increased ~75% with driving. The mean droplet trajectory angle (Fig. 8d) shows only small changes as a result of driving. Therefore, the basic fanning pattern of the droplet trajectory was nearly the same for different cases at $x = 20$ mm because the atomization and redistribution processes occurred close to the nozzle ($x < 10$ mm). The only noticeable difference was that the no-driving case has a wider central region (where $V_d \sim 0$ and $\alpha_d \sim 0$) than those of other cases.

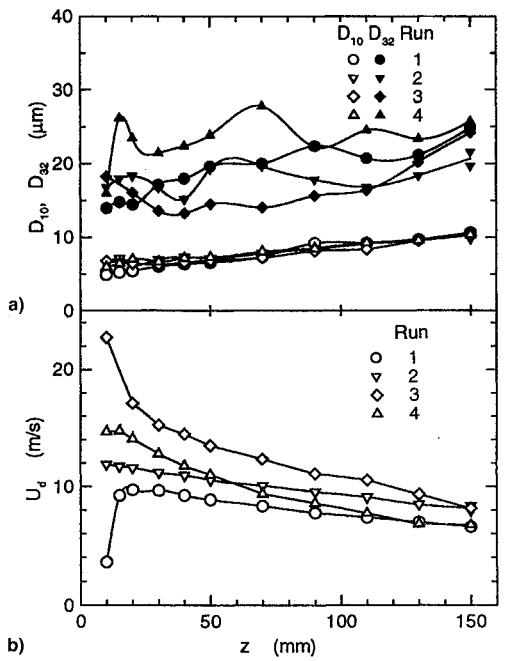


**Fig. 9 Axial profiles of a) mean droplet diameters and b) velocity components. $P_t$ = 690 kPa, $y$ = 0 mm.**

Despite the variations in the droplet velocity profiles and redistribution of droplets observed, the total liquid flow rate, measured by weighing the liquid collected in a plastic bag in a fixed time, remained nearly constant (<2%). The driver's pumping action caused increases in the mean droplet velocity and velocity perturbations, but did not alter the mean flow rate. Therefore, the substantial increase (a factor of 2–3) in the data rate in the central region, where $D_{10}$ is small, implies that a large number of small droplets were produced as a result of driving and flow in the central region. The accelerated droplet velocities observed at ~19 kHz are beneficial for a deeper penetration of droplets into the gas stream, and the redistributed spray at ~17 kHz is useful for certain applications in which uniform droplet distribution is desirable.

Figure 9 shows the axial profiles of the mean diameters and velocity components along the centerline. $D_{10}$ was nearly the same for all different conditions and increased gradually downstream. Since $D_{32}$ is more sensitive than $D_{10}$ to the occasional arrival of large droplets, it exhibits more scatter in the data points. Driving at $f \approx 19$ kHz decreased $D_{32}$ as the

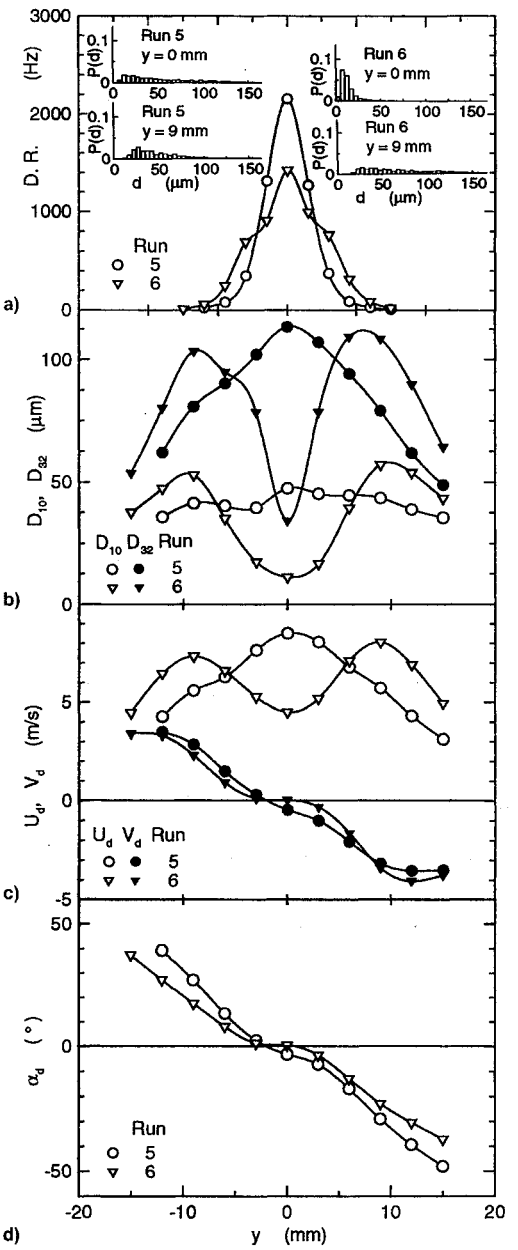


**Fig. 10 Effect of driving on the radial profiles a) data rate, b) mean droplet diameters, c) velocity components, and d) mean trajectory angle. $P_t$ = 207 kPa, $x$ = 20 mm.**

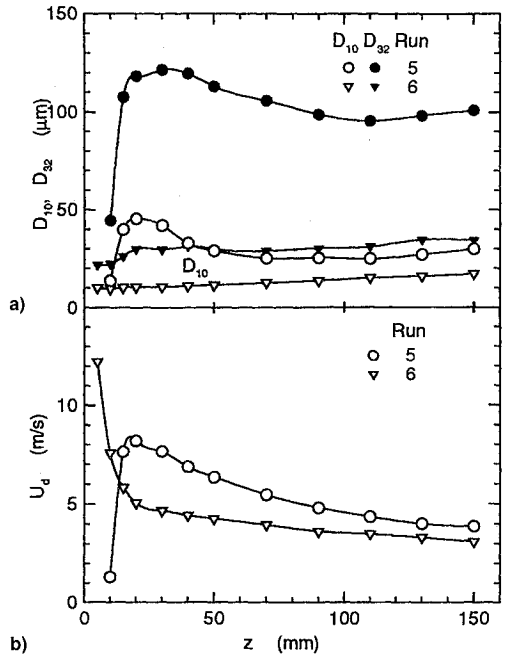


**Fig. 11 Axial profiles of a) mean droplet diameters and b) velocity components. $P_t$ = 207 kPa, $y$ = 0 mm.**

power was increased (runs 2 and 3*), except for the near-nozzle region ($x < 20$ mm), because of reduced frequencies of larger droplets. At $f \approx 17$ kHz (run 4), $D_{32}$ was larger than the no-driving case (run 1), because large droplets were thrown into the core region as a result of the bifurcated atomization. $U_d$ increased as the driving power was increased at $f \approx 19$ kHz because of the stronger pumping action. The effect of the driving frequency was insignificant (runs 2 and 4).

At a lower pressure ($P_t$ = 207 kPa), the high-power velocity modulation affected the spray structure significantly. Without driving, the conical liquid sheet became bell-shaped before atomization because of low liquid-jet momentum; thus, spray quality deteriorated. Table 1 includes $\bar{D}_{10}$ and $\bar{D}_{32}$, showing the reduction of ~17 and ~4%, respectively, as a result of driving. Figures 10b and 10c show the radial profiles of the mean droplet diameters and velocity components with and without driving at $x$ = 20 mm. For the no-driving case (run 5), $D_{10}$, $D_{32}$, and $U_d$ all exhibit a single peak on the centerline because of atomization near the center, indicating that most of the liquid mass was flowing in the core region; the spray lost its hollow-cone nature. By contrast, for run 6, the driver's pumping action assisted in forming a conical liquid sheet and atomizing it similar to the higher-pressure sprays. Consequently, the distributions of the mean diameters and velocity components became qualitatively similar to those of the high-pressure sprays, although the droplet diameters were larger and the velocity components were lower. The mean droplet trajectory angle (Fig. 10d) at a fixed $y$ became smaller with driving because the atomization point moved closer to the nozzle as the bell-shaped liquid sheet disappeared. Figure 11 shows the effect of driving on the axial profiles of $D_{10}$, $D_{32}$, and $U_d$ at $P_t$ = 207 kPa. Both $D_{10}$ and $D_{32}$ were decreased significantly by driving. Because of the difference (single peak vs double peaks) in the radial profiles of $U_d$ (Fig. 10b), $U_d$ was decreased by driving except in the near-nozzle region ($x < 15$ mm). Thus, the high-amplitude velocity modulation extends the turndown ratio by improving the spray quality, which otherwise deteriorates under low pressures.

## Conclusions

The impact of the high-amplitude velocity-modulation on the characteristics of a pressure-swirl atomizing spray is demonstrated based on the optical observations and the phase-Doppler measurements. The driver is uniquely designed to generate high-amplitude velocity perturbations rather than the mechanical vibration of the nozzle used in many other devices. As a result, a coherent roll-up of a hollow-cone liquid-sheet and subsequent uniform breakup are induced by the process similar to the impinging atomization, in a wide range of the modulation frequency (4–52 kHz). This process prevents the natural growth of the Kelvin–Helmholtz instability that otherwise develops on the conical liquid sheet, thereby reducing the liquid volume of a droplet cluster. Two distinct breakup modes exist at different resonance frequencies. At ~17 kHz, the liquid sheet atomizes and bifurcates in two major directions, thus dispersing droplets more evenly within the spray. At ~19 kHz, the spray angle narrows and the droplets in the core region accelerate as a result of the driver's pumping action. The large droplet number flux caused by the driver's pumping action is helpful in maintaining a good spray quality at low pressures and, in turn, in increasing the turndown ratio dramatically.

## Acknowledgments

This work was supported by the U.S. Air Force, Wright Laboratory, Aero Propulsion and Power Directorate, Fuels and Lubrication Division, Wright–Patterson Air Force Base, Ohio, under Contract F33615-92-C-2207 (Technical Monitor: Charles Frayne). Special thanks to T. A. Jackson for helpful discussions, G. L. Switzer for assisting in the phase-Doppler experiment, and M. Dressler and M. Best for taking photographs.

## References

[1]Lefebvre, A. H., *Gas Turbine Combustion*, Hemisphere, New York, 1983, p. 13.

[2]Locklin, D. W., "Recent Research and Development in Residential Oil Burners," *Combustion Technology: Some Modern Developments*, edited by H. B. Palmer and J. M. Beér, Academic, New York, 1974, Chap. 15.

[3]Young, J. C. O'C., Wilson, J. A., and Lang, R. J., "An Ultrasonic Oil Burner," 2nd American Petroleum Inst. Research Conf. on Distillate Fuel Combustion, API Publication 1701, Paper CP62-7, Chicago, IL, June 1962.

[4]Squire, H. B., "Investigation of the Instability of a Moving Liquid Film," *British Journal of Applied Physics*, Vol. 4, June 1953, pp. 167–169.

[5]Clark, C. J., and Dombrowski, N., "Aerodynamic Instability and Disintegration of Inviscid Liquid Sheet," *Proceedings of the Royal Society of London, Series A: Mathematical and Physical Sciences*, Vol. 329, No. 1579, 1972, pp. 467–478.

[6]Crapper, G. D., Dombrowski, N., Jepson, W. P., and Pyott, G. A. D., "A Note on the Growth of Kelvin-Helmholtz Waves on Thin Liquid Sheets," *Journal of Fluid Mechanics*, Vol. 57, No. 4, 1973, pp. 671, 672.

[7]Mansour, A., and Chigier, N., "Disintegration of Liquid Sheets," *Physics of Fluids A*, Vol. 2, No. 5, 1990, pp. 706–719.

[8]Dressler, J. L., "Two-Dimensional, High Flow, Precisely Controlled Monodisperse Droplet Source," *Aero Propulsion and Power Directorate*, Wright Lab., WL-TR-93-2049, March 1993.

[9]Wang, H. Y., McDonell, V. G., and Samuelsen, G. S., "The Two-Phase Flow Downstream of a Production Engine Combustor Swirl Cup," *Twenty-Fourth Symposium (International) on Combustion*, The Combustion Inst., Pittsburgh, PA, 1992, pp. 1457–1463.

[10]Putnam, A. A., *Combustion-Driven Oscillations in Industry*, Elsevier, New York, 1971, p. 1.

[11]Dressler, J. L., "Atomization of Liquid Cylinders, Cones, and Sheets by Acoustically Driven, Amplitude-Dependent Instabilities," International Conference on Liquid Atomization and Spray Systems, Paper 41, Gaithersburg, MD, July 1991.

[12]Dressler, J. L., "Liquid Droplet Generator," U.S. Patent 5,248,087, Sept. 28, 1993.

[13]Takahashi, F., Schmoll, W. J., and Dressler, J. L., "Characterization of a Velocity-Modulation Atomizer," *Review of Scientific Instruments*, Vol. 65, No. 11, 1994, pp. 3563–3569.

[14]Ross, F. W., McKinney, H. E., and Bjorklund, I. S., "Fluid Resonator System," U.S. Patent 3,567,185, March 2, 1971.

[15]Cha, C. L., and Hou, S. L., "Apparatus for Producing Multiple Uniform Fluid Filaments and Drops," U.S. Patent 4,138,687, Feb. 6, 1979.

[16]McDonell, V. G., and Samuelsen, S., "Sensitivity Assessment of a Phase-Doppler Interferometer to User-Controlled Settings," *Liquid Particle Size Measurement Techniques*, edited by E. D. Hirleman, W. D. Bachalo, and P. G. Felton, Vol. 2, American Society for Testing and Materials, STP 1083, 1990, pp. 170–189.

[17]Presser, C., Gupta, A. K., Avedisian, C. T., and Semerjian, H. G., "Effect of Dodecanol Content on the Combustion of Methanol Spray Flames," International Conference on Liquid Atomization and Spray Systems, Paper 56, Gaithersburg, MD, July 1991.

[18]Bachalo, W. D., Rudoff, R. C., and Sankar, S. V., "Time-Resolved Measurements of Spray Drop Size and Velocity," *Liquid Particle Size Measurement Techniques*, edited by E. D. Hirleman, W. D. Bachalo, and P. G. Felton, Vol. 2, American Society for Testing and Materials, STP 1083, 1990, pp. 209–224.

[19]Mason, B. J., Jayaratne, O. W., and Woods, J. D., "An Improved Vibrating Capillary Device for Producing Uniform Water Droplets of 15 to 500 $\mu$m Radius," *Journal of Scientific Instruments*, Vol. 40, No. 5, 1963, pp. 247–249.

[20]Ryley, D. J., and Wood, M. R., "The Construction and Operating Characteristics of a New Vibrating Capillary Atomizer," *Journal of Scientific Instruments*, Vol. 40, No. 6, 1963, pp. 303–305.

[21]Schneider, J. M., and Hendricks, C. D., "Source of Uniform-Sized Liquid Droplets," *Review of Scientific Instruments*, Vol. 35, No. 10, 1964, pp. 1349, 1350.

[22]Dabora, E. K., "Production of Monodisperse Sprays," *Review of Scientific Instruments*, Vol. 38, No. 4, 1967, pp. 502–506.

[23]Berglund, R. N., and Liu, B. Y. H., "Generation of Monodisperse Aerosol Standards," *Environmental Science and Technology*, Vol. 7, No. 2, 1973, pp. 147–153.

[24]Ibrahim, E. A., and Przekwas, A. J., "Impinging Jets Atomization," *Physics of Fluids A*, Vol. 3, No. 12, 1991, pp. 2981–2987.